

Femtosecond frequency comb measurement of absolute frequencies and hyperfine coupling constants in cesium vapor

Jason E. Stalnaker,^{1,2,*} Vela Mbele,^{2,3,†} Vladislav Gerginov,^{2,‡} Tara M. Fortier,² Scott A. Diddams,² Leo Hollberg,^{2,§} and Carol E. Tanner⁴

¹*Department of Physics and Astronomy, Oberlin College, 110 N. Professor St., Oberlin, OH 44074, USA*

²*Time and Frequency Division, National Institute of Standards and Technology, 325 Broadway MS 847, Boulder, CO 80305, USA*

³*School of Physics, University of Witwatersrand, Private Bag 3, WITS, 2050, RSA*

⁴*Department of Physics, University of Notre Dame, Notre Dame, Indiana 46556-5670, USA*

(Received 15 January 2010; published 29 April 2010)

We report measurements of absolute transition frequencies and hyperfine coupling constants for the $8S_{1/2}$, $9S_{1/2}$, $7D_{3/2}$, and $7D_{5/2}$ states in ^{133}Cs vapor. The stepwise excitation through either the $6P_{1/2}$ or $6P_{3/2}$ intermediate state is performed directly with broadband laser light from a stabilized femtosecond laser optical-frequency comb. The laser beam is split, counterpropagated, and focused into a room-temperature Cs vapor cell. The repetition rate of the frequency comb is scanned and we detect the fluorescence on the $7P_{1/2,3/2} \rightarrow 6S_{1/2}$ branches of the decay of the excited states. The excitations to the different states are isolated by the introduction of narrow-bandwidth interference filters in the laser beam paths. Using a nonlinear least-squares method we find measurements of transition frequencies and hyperfine coupling constants that are in agreement with other recent measurements for the $8S$ state and provide improvement by 2 orders of magnitude over previously published results for the $9S$ and $7D$ states.

DOI: [10.1103/PhysRevA.81.043840](https://doi.org/10.1103/PhysRevA.81.043840)

PACS number(s): 42.62.Fi, 42.62.Eh, 32.30.-r, 32.10.Fn

I. INTRODUCTION

The basic ideas of using repetitive pulses and mode-locked lasers for high-resolution precision spectroscopy were originally developed in the 1970s, with particular focus on Doppler-free two-photon transitions [1–6]. The advent of fully stabilized optical frequency combs [7,8] in 2000 renewed interest in many spectroscopic applications of mode-locked lasers (for a review see Ref. [9]). In many instances the use of direct frequency-comb spectroscopy (DFCS) offers many advantages over spectroscopy done with cw lasers. In particular, the spectral versatility provided by modern frequency combs allows the simultaneous study of multiple atomic transitions with a single experimental setup. Additionally, DFCS allows for a relatively simple determination of the absolute frequency by providing a direct link to the System of International Units second. In this work we exploit this versatility to study multiple transitions in cesium (Cs).

Precision spectroscopy of Cs plays an important role in atomic and fundamental physics, including measurements of atomic parity violation [10–12], searches for the permanent electric dipole moment of an electron [13,14], photon recoil measurements that help determine the fine structure constant [15,16], measurements of the distribution of nuclear charge and magnetization [17], and numerous applications in laser cooling, Bose-Einstein condensation [18], atomic clocks [19], and magnetometers [20].

The present work focuses on measuring multiple transition frequencies and the hyperfine structure of select low-lying states in cesium via two-photon excitation. The relatively simple experimental setup uses a room-temperature Cs vapor cell and a self-referenced optical frequency comb to excite Doppler-free two photon transitions from the Cs ground state to the $8S_{1/2}$, $9S_{1/2}$, $7D_{3/2}$, and $7D_{5/2}$ states. Our results are consistent with previous measurements for the well-studied $8S_{1/2}$ state [21,22] and provide significantly reduced uncertainties for the $9S_{1/2}$, $7D_{3/2}$, and $7D_{5/2}$ states [23].

This article is structured as follows: Sec. II contains a description of our experimental system and measurements. In Sec. III we examine the features of the fluorescence spectra and discuss the theoretical model used to describe the results. Section IV describes the analysis of the two-photon transitions and the recipe used in extracting the transition energies. This section also includes our results and the details of the systematic effects. We conclude our work in Sec. V.

II. EXPERIMENTAL SETUP

The relevant Cs energy levels are shown in Fig. 1. The excitation pathways to the four states $8S_{1/2}$, $9S_{1/2}$, $7D_{3/2}$, or $7D_{5/2}$ proceed through a stepwise excitation through either the $6P_{1/2}$ or the $6P_{3/2}$ states. We detect the two-photon excitation as blue fluorescence emission as the atoms decay from the $7P_{1/2,3/2}$ states to the ground state.

The experimental setup is shown in Fig. 2. We excite the cascaded two-photon transitions using a mode-locked Ti:sapphire laser that generates a broad optical frequency comb. The portion of the output spectrum that was used extended from 650 to 1000 nm, covering all of the excitation transitions of interest in Fig. 1. The laser is described in detail in Ref. [24] and here we only briefly mention the information relevant for the experiment. The Kerr-lens

*Corresponding author: jason.stalnaker@oberlin.edu

†Present address: P. O. Box 755, Durban, KwaZulu Natal, 4000, Republic of South Africa.

‡Present address: Physikalisch-Technische Bundesanstalt, Bundesallee 100, 38116, Germany.

§Present address: P. O. Box 60157, Sunnyvale, CA 94088, USA.

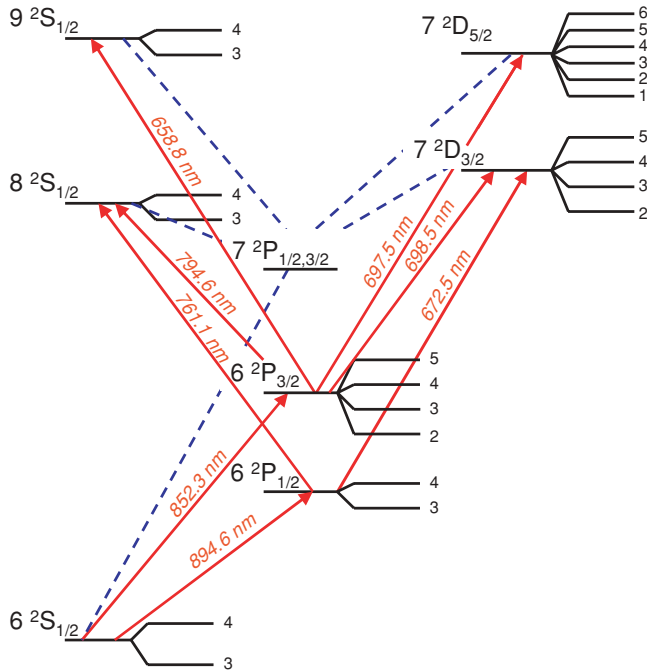


FIG. 1. (Color online) Energy levels of ^{133}Cs ($I = 7/2$) that are relevant to this work. The excitation pathways are shown in solid red along with the transition wavelengths. The decay channels used in the detection are shown in blue dashed lines. The total angular momentum of the hyperfine components is listed next to each state.

mode-locked Ti:sapphire ring laser produces an output spectrum consisting of discrete equally spaced coherent optical modes. The frequency of each optical mode, ν_n , can be related to two microwave frequencies, the laser repetition rate, f_{rep} , and the carrier-envelope offset frequency, f_0 , by

$$\nu_n = n f_{\text{rep}} + f_0, \quad (1)$$

where n is an integer mode number $\sim 4 \times 10^5$. The carrier-envelope-offset frequency is stabilized by use of an f -to- $2f$ interferometer, thus “self-referencing” all modes of the comb [7]. For the measurements described here f_0 was stabilized to 45 MHz. The repetition rate of the laser was ≈ 1 GHz. The

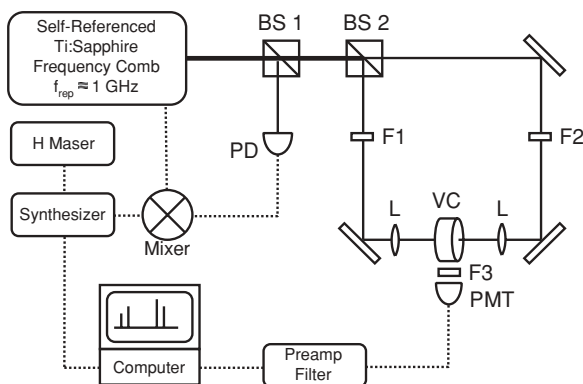


FIG. 2. Block diagram of the experimental setup. The components are the following: BS 1 and BS 2, nonpolarizing beam splitters; F1, F2, and F3, interference filters; L, lens; PD, photodiode; PMT, photomultiplier tube; VC, Cs vapor cell.

repetition rate was phase locked to a signal generator that was referenced to a hydrogen maser. With the comb stabilized in this way, the fractional instability of every optical frequency of the comb is $\approx 2 \times 10^{-13} \tau^{-\frac{1}{2}}$, where τ is the averaging period in seconds.

The laser beam was split by use of a 50-50 nonpolarizing beam-splitting cube (BS 2). The two output laser beams were linearly polarized along the same axis. The beams were filtered by use of either narrowband interference filters or a combination of long-pass and short-pass filters to select specific transition pathways. The counterpropagating beams were then focused by lenses with focal lengths of 25 cm to a spot size of $\sim 100\ \mu\text{m}$ inside the vapor cell. Focusing the beams to a smaller waist size increases the two-photon excitation rate, but also leads to broadening of the resonances due to the finite transit-time of the atoms through the beams. The transit-time broadening for a waist of this size is about 2 MHz for room-temperature Cs atoms. The average optical intensities in the vapor cell were tens of W/cm^2 spread over an ≈ 10 -nm bandwidth, corresponding to ≈ 4000 optical frequencies.

An evacuated Pyrex Cs vapor cell was used in the experiment. The cell had a diameter of 2.5 cm and was a wedge shape with an optical path length ranging from 0.5 to 1 cm. Windows were fused directly to the cell at an angle. The cell was carefully cleaned and filled in an oil-free vacuum system and was evacuated to a base pressure of $\sim 10^{-5}$ Pa. A small amount of Cs was introduced into the cell prior to removing it from the vacuum system. The cell temperature was varied by resistive heater wires wound around the cell. We note that we observed shifts in the transition frequencies as large as 0.5 MHz in a Cs vapor cell that was not cleaned and vacuum processed as carefully as the cell used in these measurements.

Most of the measurements in this experiment were taken with the Cs cell temperature at 297 K, with fluctuations less than 1 K. Data were taken at higher temperatures to evaluate systematic shifts arising from pressure shifts as described in Sec. IV B.

A set of six coils was used to zero out the earth’s magnetic field in the region of the vapor cell. The field was reduced to a level of $< 1\ \mu\text{T}$ over the interaction region inside the vapor cell.

Two-photon resonance signals were monitored by measuring the $7P_J \rightarrow 6S_{1/2}$ ($J = 1/2, 3/2$) cascade fluorescence at 459 and 455 nm. The fluorescence was collected at a right angle to the two counterpropagating beams and was detected by a photomultiplier tube. The detector was shielded from background light and the scattered light from the excitation laser beams by a 457.9-nm filter with a 10-nm pass band (F3). The detector output was amplified and filtered (low-pass at 1 kHz, 6 dB/octave) before being sampled and recorded with a computer-controlled data acquisition board (DAQ).

The DAQ used in these measurements is similar to that used in Refs. [16,17,25]. The computer controlled the scan of the repetition rate by stepping the frequency of the signal generator to which the repetition rate was phase locked. Data scans were collected by changing the frequency of the signal generator from 1000.771 725 to 1000.774 725 MHz in 1-Hz steps. This 3-kHz range in the repetition rate results in a

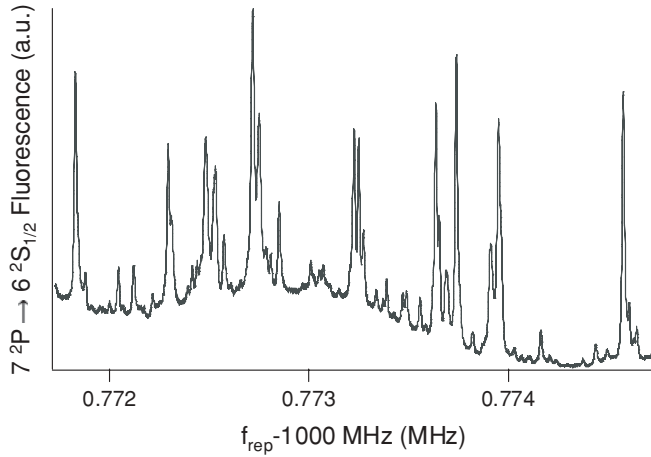


FIG. 3. Fluorescence from the $7P_J \rightarrow 6S_{1/2}$ decay as a function of laser repetition rate when no filters (F1 and F2 in Fig. 2) are used to restrict the laser's spectral bandwidth.

2- to 3-GHz variation in the two-photon frequency, depending on the transition. At each 1-Hz step the fluorescence was digitized with multiple samples and averaged for 1 s. The statistical mean and the uncertainty in the mean were evaluated at each repetition rate frequency. Spectra were collected for both increasing and decreasing frequency scans, resulting in 6002 data points.

III. OBSERVED SPECTRA AND THEORETICAL CONSIDERATIONS

Figure 3 shows the spectrum collected as the repetition rate of the frequency comb was scanned without using the filters marked as F1 and F2 in Fig. 2. The spectrum consists of a multitude of narrow Doppler-free peaks and a Doppler-broadened background. The narrow peaks are due to excitation to the $8S$, $9S$, and $7D$ states by two counterpropagating photons, while the Doppler-broadened background is due to excitation from two copropagating photons. The observed spectrum is quite complicated because of the numerous discrete frequencies present in the comb combined with the multiple atomic energy levels and accessible transition pathways.

The spectrum is greatly simplified and the Doppler background is eliminated by introducing filters F1 and F2, as shown in Fig. 2. The presence of the filters restricts the transitions and enables the selection of individual excitation pathways. Figure 4 shows the spectrum observed when one of the counterpropagating laser beams is restricted to be between 845 and 855 nm and the other between 780 and 800 nm. With this combination, the first beam can excite the atoms on only the $6S_{1/2} \rightarrow 6P_{3/2}$ transition at 852 nm (the D_2 transition) and the second beam can only excite the atoms on the $6P_{3/2} \rightarrow 8S_{1/2}$ transition at 795 nm. This eliminates excitations to the $9S_{1/2}$, $7D_{3/2}$, and $7D_{5/2}$ states, as well as the excitation to the $8S_{1/2}$ state through the $6P_{1/2}$ state, and removes the Doppler-broadened background. The resulting spectrum consists of groups of two or three peaks. The peaks labeled d, e, and f form one such spectral group and are shown in more detail in Fig. 5. Each spectral group is the result of

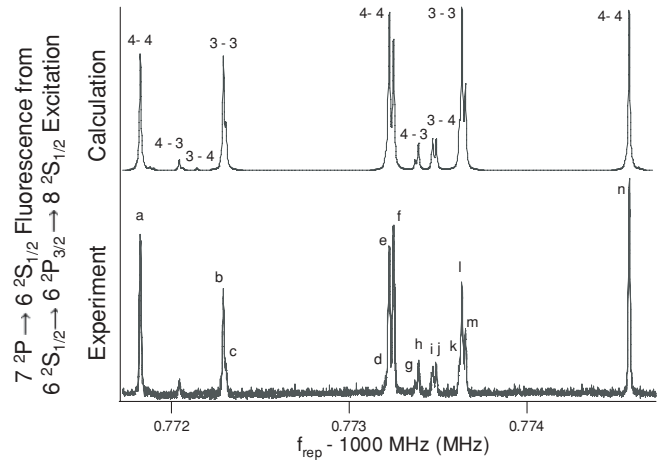


FIG. 4. The calculated spectrum (upper trace) and experimental signal (lower trace) of the $7P \rightarrow 6S$ fluorescence when the Cs atoms are excited to the $8S_{1/2}$ state through the $6P_{3/2}$ state. The groups of peaks in the calculated spectrum are labeled by $F-F''$ to denote the hyperfine ground state and the hyperfine final state of the transition. The peaks in each group correspond to the different hyperfine components of the intermediate state. The peaks in the experimental spectrum that are labeled with letters were used in extracting the transition frequencies, as described in the text.

excitation from a given ground-state hyperfine level to a given excited-state hyperfine level, and the individual peaks in the group correspond to specific transition pathways through every allowable hyperfine level of the intermediate state. For example, the d, e, and f peaks in Fig. 5 all correspond to excitation from the $6S_{1/2}$ ($F=4$) ground state to the $8S_{1/2}$ ($F''=4$) excited state. The three peaks correspond to excitation through the $6P_{3/2}$ ($F'=3,4,5$) intermediate states. We see the groups recur as a different pair of optical modes is resonant with a given transition. This repeating pattern occurs at intervals of $\delta f_{\text{rep}} \approx 1.2$ kHz, corresponding to a change in the two-photon optical frequency of ≈ 1 GHz (i.e., the laser mode spacing). For a given group of three peaks there

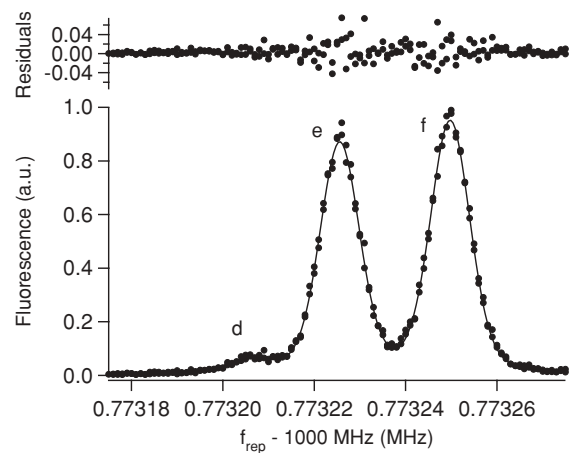


FIG. 5. The $7P \rightarrow 6S$ fluorescence when the Cs atoms are excited to the $8S_{1/2}$ state through the $6P_{3/2}$ state. The peaks correspond to the d, e, and f peaks in Fig. 4. This data set was taken at a temperature of 319 K and was used in evaluating systematic effects related to temperature dependence.

are three different velocity classes that satisfy the resonance condition for each of the corresponding hyperfine components of the intermediate level. For another group of three peaks, the resonant condition for the components of the intermediate level is satisfied by a different pair of comb modes and by different velocity classes. Thus, the amplitudes of the peaks arising from the same ground, excited, and intermediate states are not the same in the different spectral groups.

We can understand and calculate the spectra using the standard two-photon transition probabilities derivable from

second-order time-dependent perturbation theory. We start by considering a transition of an atom in the ground state with total angular momentum F , $|6S_{1/2} F\rangle$, to an excited state with total angular momentum F'' , $|n''L''_{J''} F''\rangle$, via excitation by two cw lasers with angular frequencies ω_1 and ω_2 , intensities I_1 and I_2 , and wave vectors \vec{k}_1 and \vec{k}_2 . Here n'' refers to the principal quantum number of the excited state. We further assume that ω_1 is close to the resonant frequency for the $6S_{1/2} \rightarrow 6P_{J'}$ transition, with $J' = 1/2$ or $3/2$. The probability of the atom to make a transition is [26]

$$P(6S_{1/2}F, n''L''_{J''}F'') \propto \frac{1}{2F+1} \frac{I_1 I_2}{[\omega_{6S_{1/2}F:n''L''_{J''}F''} - (\omega_1 + \vec{k}_1 \cdot \vec{v}) - (\omega_2 + \vec{k}_2 \cdot \vec{v})]^2 + \left(\frac{\gamma_{n''L''_{J''}}}{2}\right)^2} \times \sum_{M_F, M_F''} \left| \sum_{F', M_F'} \frac{\langle n''L''_{J''}F'' M_F'' | \hat{e}_2 \cdot \vec{d} | 6P_{J'}F'M_F' \rangle \langle 6P_{J'}F'M_F' | \hat{e}_1 \cdot \vec{d} | 6S_{1/2}FM_F \rangle}{\omega_{6S_{1/2}F:6P_{J'}F'} - (\omega_1 + \vec{k}_1 \cdot \vec{v}) - i\frac{\gamma_{6P_{J'}}}{2}} \right|^2, \quad (2)$$

where \vec{v} is the velocity of the atom; M_F , M_F' , and M_F'' are the projections of the total angular momenta F , F' , and F'' along the axis of quantization; \vec{d} is the electric dipole operator; $\hat{e}_{1(2)}$ is the unit vector along the direction of the polarization for the first (second) laser beam; γ_{nL_J} is the homogeneous linewidth of the state $|nL_J\rangle$; and $\omega_{nL_JF:n'L'_JF'}$ is the resonant angular frequency of the transition $|nL_JF\rangle \rightarrow |n'L'_JF'\rangle$. For a given light polarization, specified by the vector component in the spherical basis q , the matrix elements for the different magnetic sublevels can be related to reduced matrix elements that do not depend on the magnetic sublevels or the total angular momentum (F , F' , or F'') by use of the Wigner-Eckart theorem and standard Clebsch-Gordan relations as [27]

$$\begin{aligned} & \langle n'L'_JF'M_F' | d_q | nL_JFM_F \rangle \\ &= (-1)^{F'-M_F'} \begin{pmatrix} F' & 1 & F \\ -M_F' & q & M_F \end{pmatrix} \langle n'L'_JF' || d || nL_JF \rangle \\ &= (-1)^{F'-M_F'+I+1+J+F} \sqrt{(2F+1)(2F'+1)} \\ & \times \begin{pmatrix} F' & 1 & F \\ -M_F' & q & M_F \end{pmatrix} \begin{Bmatrix} J' & F' & I \\ F & J & 1 \end{Bmatrix} \langle n'L'_JF' || d || nL_J \rangle. \end{aligned} \quad (3)$$

Here $I = \frac{7}{2}$ is the nuclear spin and the $()$ and $\{ \}$ terms are the usual 3- J and 6- J symbols. Thus, the transition probabilities for different ground-state angular momenta F and excited-state angular momenta F'' can be related to a common factor by use of the appropriate Clebsch-Gordan coefficients. If we assume the two laser beams are counterpropagating, then examination of Eq. (2) reveals that, for a given transition from the ground state with angular momentum F , through an intermediate state with angular momentum F' , to a final state with F'' , the transition probability will be a maximum when

$$\omega_1 \left(1 + \frac{v}{c}\right) + \omega_2 \left(1 - \frac{v}{c}\right) = \omega_{6S_{1/2}F:n''L''_{J''}F''} \quad (4)$$

and

$$\omega_1 \left(1 + \frac{v}{c}\right) = \omega_{6S_{1/2}F:6P_{J'}F'}. \quad (5)$$

If we now consider the effect of having a number of discrete frequencies coming from the different modes of the comb, we see that, as a result of the detuning from the intermediate state, only two near-resonant comb modes will contribute substantially to the transition probability. Because the spacing of the frequencies for the comb, $f_{\text{rep}} \approx 1$ GHz, is much larger than the homogeneous linewidths of the states, $\frac{\gamma}{2\pi} \approx 5$ MHz, we are justified in considering only the two modes closest to the resonance conditions of Eqs. (4) and (5). Since these two frequencies are coming from the comb, they are related to the offset frequency and repetition rate of the comb by two integers as

$$\omega_1 = 2\pi(f_0 + n_1 f_{\text{rep}}), \quad (6)$$

$$\omega_2 = 2\pi(f_0 + n_2 f_{\text{rep}}). \quad (7)$$

Substituting these relations into Eqs. (4) and (5) we see that for a given pair of modes, n_1 and n_2 , and a fixed value of the offset frequency there exists a unique repetition-rate frequency and velocity that will simultaneously satisfy both resonance conditions. Therefore, given an atomic sample with a broad enough velocity distribution, there will exist a repetition-rate frequency that will result in a stepwise resonant excitation of the two-photon transition for a specific velocity class. This leads to the narrow Doppler-free peaks seen in Fig. 4. Because the velocity class excited and the resonant repetition-rate frequency both depend on the energy of the intermediate state, the transition resonance for each different intermediate state occurs at different repetition rates. Because a different velocity class contributes to the different peaks, the amplitudes of the peaks vary greatly, depending on the number of atoms that are present in the resonant velocity class.

IV. ANALYSIS AND RESULTS

A. Analysis

We calculated the excitation probabilities by numerically integrating Eq. (2) over a Gaussian velocity distribution for optical modes near the resonant condition. A total of ≈ 15 optical modes were used (10 for the first-stage excitation and 5 for the second-stage excitation). The calculated spectra agree quite well with the experimental spectra (Fig. 4). Slight variations in the relative amplitudes of the peaks are attributed to slight deviations of the polarization of the excitation light from linear.

The resonant frequencies for a transition from a ground state with a specific F to an excited state with F'' are related to the center-of-gravity frequencies and the hyperfine coupling constants through (see, e.g., [28])

$$\begin{aligned} & \nu_{6S_{1/2}F:n''L''_{j''}F''} \\ &= \nu_{6S_{1/2:n''L''_{j''}} - \frac{1}{2}A_{6S_{1/2}}\kappa(F, J) + \frac{1}{2}A_{n''L''_{j''}}\kappa(F'', J'') + B_{n''L''_{j''}} \\ & \quad \times \frac{\frac{3}{4}\kappa(F'', J'')^2 + \frac{3}{4}\kappa(F'', J'') - I(I+1)J''(J''+1)}{2I(2I-1)J''(2J''-1)}, \end{aligned} \quad (8)$$

where $\kappa(F, J) = F(F+1) - I(I+1) - J(J+1)$.

The repetition rates at which the calculated resonances occur depend on the center-of-gravity frequencies for the two stages of the excitation and the hyperfine A and B constants of the ground, intermediate, and final states. Spectra were calculated with different values of the two-photon center-of-gravity frequency and hyperfine coupling constants of the final excited state. The intermediate state energy and coupling constants used in the calculated spectra were fixed to the values determined from Gerginov *et al.* [16,25]. The two-photon transition center-of-gravity frequencies $\nu_{6S_{1/2:n''L''_{j''}}$ and the hyperfine coupling constants $A_{n''L''_{j''}}$ and $B_{n''L''_{j''}}$ were extracted from the experimental data by least-squares comparison of the experimental resonant repetition-rate frequencies with the resonant repetition-rate frequencies determined from the calculated spectra.

The resonant repetition rate for each of the peaks in both the experimental and the calculated spectra were determined from a least-squares fit. Fitting the spectra was necessary in order to account for the overlap of the different peaks. The calculated spectra were assumed to have a Lorentzian line shape. However, the experimental spectra were found to be well described by a line shape of a Gaussian coupled to a Lorentzian,

$$\sum_i \left(C_i^G e^{-\frac{(f-f_i)^2}{2\gamma_G^2}} + C_i^L \frac{\left(\frac{\gamma_L}{2}\right)^2}{(f-f_i)^2 + \left(\frac{\gamma_L}{2}\right)^2} \right) + C^B, \quad (9)$$

where C_i^G and C_i^L are the Gaussian and Lorentzian amplitudes, respectively, γ_G and γ_L are the Gaussian and Lorentzian widths, f_i is the line center of the i^{th} peak, and C^B is a constant baseline offset. We attribute the deviation of the experimental line shape from the expected Lorentzian line shape to residual misalignment of the two beams, which we discuss further later in this article. We designate the resonant repetition-rate frequency for the i^{th} peak determined by fitting

the calculated spectra for a given $\nu_{6S_{1/2:n''L''_{j''}}$, $A_{n''L''_{j''}}$, and $B_{n''L''_{j''}}$ by $f_i^{\text{calc}}(\nu_{6S_{1/2:n''L''_{j''}}, A_{n''L''_{j''}}, B_{n''L''_{j''}})$. The resonant repetition-rate frequencies determined from the experimental spectra we designate as f_i^{expt} . The best-fit values for two-photon frequency and the hyperfine constants were determined by minimizing the weighted χ^2 function,

$$\begin{aligned} & \chi^2(\nu_{6S_{1/2:n''L''_{j''}}, A_{n''L''_{j''}}, B_{n''L''_{j''}}) \\ &= \sum_i \left(\frac{f_i^{\text{expt}} - f_i^{\text{calc}}(\nu_{6S_{1/2:n''L''_{j''}}, A_{n''L''_{j''}}, B_{n''L''_{j''}})}{\sigma_i^{\text{expt}}} \right)^2, \end{aligned} \quad (10)$$

with respect to $\nu_{6S_{1/2:n''L''_{j''}}$, $A_{n''L''_{j''}}$, and $B_{n''L''_{j''}}$. Here σ_i^{expt} is the standard uncertainty in f_i^{expt} determined by the fit to the experimental data. For N peaks and all three parameters ($\nu_{6S_{1/2:n''L''_{j''}}$, $A_{n''L''_{j''}}$, and $B_{n''L''_{j''}}$) one would expect the minimum value of the χ^2 to be $N - 3$. We consistently observed larger values of the χ^2 . We attribute this uncertainty to residual misalignment, which will be discussed in more detail later. In order to account for this larger χ^2 value, we normalize the χ^2 function so that its minimum corresponds to the expected value. We then determine the uncertainty in the two-photon optical frequency and the hyperfine coupling constants by finding the values of $\nu_{6S_{1/2:n''L''_{j''}}$, $A_{n''L''_{j''}}$, and $B_{n''L''_{j''}}$, where the normalized χ^2 function increases by 1 from the point at which it is a minimum. This amounts to increasing the uncertainty to make the frequencies extracted from the different peaks self-consistent.

B. Results for the $8S_{1/2}$ state

The spectral range of the comb allowed the $8S_{1/2}$ state to be studied by use of transitions through either the $6P_{1/2}$ (895 and 761 nm) or the $6P_{3/2}$ (852 and 795 nm) states. This redundancy provided a check for consistency of the measurement and the parameter extraction method. A complete study of the systematics was performed only for the transitions that occurred through the $6P_{3/2}$ states.

Figure 6 shows the spectrum for the $6S_{1/2} \rightarrow 6P_{1/2} \rightarrow 8S_{1/2}$ transition along with the calculated spectrum. The spectrum was collected by the use of a 890-nm filter with a 10-nm passband for F1 and a combination of a 755-nm filter with a 40-nm passband with a long-pass filter at 715 nm for F2. The 13 peaks, labeled a through m in Fig. 6, were used to extract the transition frequencies. The peaks were acquired with both increasing and decreasing scans of f_{rep} , resulting in 26 individual peaks. By use of the procedure described previously, the extracted center-of-gravity two-photon frequency and the hyperfine A constant for the $8S_{1/2}$ state were found to be 729 009 798.844(38) and 219.137(19) MHz. The χ^2 was 31 for 26 peaks. Here the uncertainties are determined from the χ^2 function, as described in Sec. IV A, and do not include any systematic uncertainties.

The $6S_{1/2} \rightarrow 6P_{3/2} \rightarrow 8S_{1/2}$ transition is shown in Fig. 4. For this spectrum, one of the counterpropagating laser beams was filtered with an interference filter centered at 850 nm with a 10-nm passband. This resulted in an average intensity of ≈ 60 W/cm² in the interaction region, spread over ≈ 4000 optical modes. This light served to excite the first step of the

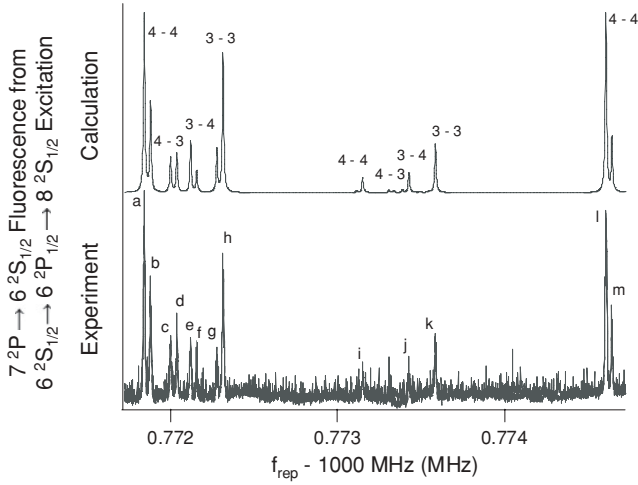


FIG. 6. The calculated spectrum (upper trace) and experimental signal (lower trace) of the $7P \rightarrow 6S$ fluorescence when the Cs atoms are excited to the $8S_{1/2}$ state through the $6P_{1/2}$ state. The peaks in the experimental spectrum that are labeled with letters were used in extracting the transition frequencies as described in the text.

two-photon transition at 852 nm. Based on the transmission profile of the filter we estimate that we have $\approx 10 \text{ mW/cm}^2$ of light in the optical mode resonant with the $6S_{1/2} \rightarrow 6P_{3/2}$ transition. The second stage of the transition was selected by use of a combination of a 800 nm short-pass filter and a 780 nm long-pass filter and provided $\approx 70 \text{ W/cm}^2$ over ≈ 8000 modes. Using the procedure described above we fit the 14 peaks labeled in the figure and find a center-of-gravity frequency of $729\,009\,798.863(29) \text{ MHz}$ and a hyperfine coupling constant $219.133(17) \text{ MHz}$, where again, the uncertainties are determined purely from the χ^2 function. The value of the χ^2 was 64 for 28 peaks (14 peaks from both the increasing and decreasing frequency scans) prior to the normalization. As described in Sec. IV A the uncertainties are increased to make the χ^2 consistent with the expected value. The resulting frequencies are in good agreement with the value extracted from the transition through the $6P_{1/2}$ state.

We analyzed in detail the systematic effects that could lead to a shift of the measured frequencies from the true transition frequencies using the transitions to the $8S_{1/2}$ state through the $6P_{3/2}$ state. Systematic shifts might be more significant for excitation through the $6P_{3/2}$ state, because of the smaller hyperfine structure shifts of the $6P_{3/2}$ state, relative to the $6P_{1/2}$ state. In addition, the signal-to-noise ratio of the spectrum

excited through the $6P_{3/2}$ state was higher than that excited through the $6P_{1/2}$ state, as an artifact of the filters used in the measurements.

We considered four possible sources of systematic effects: ac Stark shifts, Zeeman shifts, pressure shifts, and errors arising from misalignment of the counterpropagating laser beams. The associated uncertainties are summarized in Table I and described subsequently.

To evaluate the systematics we focused on the peaks labeled d, e, and f in Fig. 4. A typical data set and fit to the peaks is shown in Fig. 5. The effect of ac Stark shifts on the extracted frequencies was investigated by varying the optical powers. Neutral density filters were used to reduce the power in both beams by approximately the same amount. Data were collected at three optical powers ranging from the maximum power, which was used for collection of the full spectrum shown in Fig. 4, to 60% of the maximum power. The three peaks used in this analysis correspond to the $6S_{1/2} (F = 4) \rightarrow 6P_{3/2} (F' = 3, 4, 5) \rightarrow 8S_{1/2} (F'' = 4)$ transitions. Because the final state is the same for all three peaks, it is not possible to extract both the center-of-gravity frequency and the hyperfine A constant from these data. In order to place a limit on possible effects due to the ac Stark shifts on the center-of-gravity frequency, we fixed the hyperfine A constant to the value determined from the analysis of the full spectrum and then extracted a center-of-gravity frequency at each power by finding the minimum in the χ^2 function as defined by Eq. (10). The center-of-gravity frequencies as a function of power were fitted to a straight line. We used the slope of the line to look for any possible dependence of the center-of-gravity frequency on the power. We find the slope to be $-43(123) \text{ kHz}/P$, where P is the normalized operating power. Combining the value of the slope with its uncertainty we arrive at a maximum possible shift of 166 kHz at the nominal operating power, $P = 1$. We take this value as an estimate of the systematic uncertainty from the ac Stark effect. Because we fix the hyperfine A constant this approach provides an upper limit on the center-of-gravity frequency. Therefore, we do not attempt to apply a correction to the data. To determine the possible effect on the hyperfine splitting we fix the center-of-gravity frequency to the value determined from the analysis of the full spectrum and extract the hyperfine A constant from the data. Fitting the data for the A constant we find a slope of $-22(72) \text{ kHz}/P$, resulting in an uncertainty of 94 kHz.

For two-photon transitions between S states with $\Delta M_F = 0$ there is no linear Zeeman shift. However, the laser polarization

TABLE I. Summary of the contributions to the error budget for the measured transition frequencies and hyperfine constants. All frequencies are given in kilohertz.

Effect	$\nu_{6S_{1/2}:8S_{1/2}}$	$A_{8S_{1/2}}$	$\nu_{6S_{1/2}:9S_{1/2}}$	$A_{9S_{1/2}}$	$\nu_{6S_{1/2}:7D_{3/2}}$	$A_{7D_{3/2}}$	$B_{7D_{3/2}}$	$\nu_{6S_{1/2}:7D_{5/2}}$	$A_{7D_{5/2}}$	$B_{7D_{5/2}}$
ac Stark	166	94	169	79	49	14	17	85	11	458
B field	70	40	18	7	17	3	17	35	6	125
Cs vapor pressure	31	18	34	15	12	1	26	7	1	38
Alignment	22	20	58	20	48	12	143	34	7	180
Overlap of $7D_{3/2}$	–	–	–	–	–	–	–	9	1	30
Statistical	24	13	58	30	28	20	72	25	4	86
Total	186	106	192	88	77	15	164	102	15	517

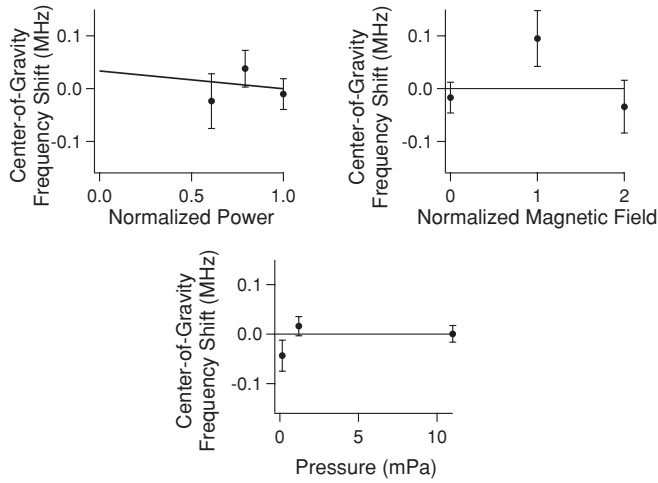


FIG. 7. The dependence of the center-of-gravity frequencies for the $6S_{1/2} \rightarrow 6P_{3/2} \rightarrow 8S_{1/2}$ state on the power (upper left), the magnetic field (upper right), and the Cs vapor pressure (bottom). The straight line for the power dependence is a weighted linear fit to the data. The vertical axis has been offset and centered so that the nominal operating point is at zero for the power-dependence plot. The magnetic field and pressure data are shown scattered about the weighted mean of the data. The horizontal axis for the power dependence is plotted as a function of the fraction of the maximum power. The horizontal axis for the magnetic field dependence is plotted as a function of the residual magnetic field, $\approx 50 \mu T$.

is not perfectly linear and these states are stepwise resonant through the intermediate P states, which are magnetically sensitive. In addition, the power on the first stage of the transition is near saturation, so there may be some optical pumping that could couple with an external magnetic field to lead to asymmetric line shapes. To investigate the effect of Zeeman shifts due to imperfect cancellation of stray magnetic fields, data were collected without the compensation coils and also with the current through the compensation coils reversed, thus doubling the residual magnetic field. Again, the peaks labeled d, e, and f in Fig. 4 were used. The value of the hyperfine A constant was fixed and the center-of-gravity frequency was extracted as described above. We see no evidence for a systematic shift as the magnetic field is increased (Fig. 7). The standard deviation of the data is 70 kHz, which we take as the uncertainty associated with the magnetic field. A similar analysis for the hyperfine A constant (with the center-of-gravity frequency fixed) also shows no evidence of any shift with the magnetic field. Using the standard deviation of the points shown in Fig. 7 as an estimate of the uncertainty we assign a 40-kHz uncertainty to the A constant due to possible magnetic fields.

For an analysis of the shifts due to collisions, the pressure of the Cs vapor was changed by heating the vapor cell as described previously. Data were taken at temperatures of 297, 318.6, and 345.5 K, corresponding to Cs vapor pressures of 0.15, 1.2, and 11 mPa. As described previously, we determine the center-of-gravity frequency with a fixed hyperfine A constant for each pressure. We see no indication of any variation of the data with the Cs vapor pressure (Fig. 7). The standard deviation

of the frequencies extracted at the different temperatures is 31 kHz, which we take as the uncertainty in the center-of-gravity frequency due to temperature or pressure effects. For the hyperfine A constant, the scatter in the data taken at different temperatures gives a standard deviation of 18 kHz, which we adopt as the uncertainty.

The final systematic considered was possible error due to imperfect alignment of the counterpropagating laser beams. The effect of misalignment of the two beams is to broaden and shift the peaks through a first-order Doppler shift. As can be seen from Eq. (2), the position of the peaks depends on the difference in the magnitude and direction of the two vectors \vec{k}_1 and \vec{k}_2 as well as the velocity class excited. Additional first-order Doppler shifts come into play if the wave fronts of \vec{k}_1 and \vec{k}_2 are not precisely counterpropagating, which can result from divergence of the counterpropagating beams and mismatch of the spatial modes. For a spectrum that contains many peaks coming from many different velocity classes the shift due to the misalignment largely averages out. This effect was investigated theoretically by modifying the program to include the effect of misalignment of the two beams. This was done by changing the $\vec{k}_2 \cdot \vec{v}$ term in Eq. (2) to include an additional perpendicular velocity component. For the $8S$ state three spectra were calculated with different angles of misalignment. Analysis of the calculated spectrum and an estimate of the maximum possible misalignment of the beams gives a conservative limit on possible effects from angular misalignment of 22 kHz for the center-of-gravity frequency and 20 kHz for the hyperfine A constant. If we attribute the scatter in the experimental results to angular misalignment, we conclude that for all the spectra the effective angular deviation due to either misalignment or to divergence and mode mismatch of the beams is less than 0.04 rad. We note that for the calculated data the misalignment of the counterpropagating laser beams leads to no significant shift in the extracted frequency; however, it does lead to a larger spread of the data and an increased value of χ^2 , as observed. This additional spread of the data beyond what is expected from the statistical noise is taken into account by conservatively increasing the uncertainties to achieve the expected χ^2 , as described in Sec. IV A.

In addition, the effect of misalignment on the $6S_{1/2} \rightarrow P_{1/2} \rightarrow 7D_{3/2}$ transition was investigated experimentally. The study of this transition confirmed that while the individual peaks did shift, there was no shift in the mean value of the transition frequency, within the uncertainty of our measurement.

The nonzero second-order Doppler shift $(v/c)^2 v_0$ is about 300 Hz for this transition and is negligible compared to the other uncertainties.

Table I summarizes the corrections and associated uncertainties of the extracted center-of-gravity and hyperfine A constants. We see no evidence for any shift that is larger than the uncertainty associated with evaluating the effect. As our final value we take the mean of the $8S_{1/2}$ frequencies determined from the $6P_{1/2}$ and $6P_{3/2}$ intermediate states, weighted by their respective statistical uncertainties, and apply the corrections and systematic uncertainties (propagated in quadrature) listed in Table I. We find final values for the

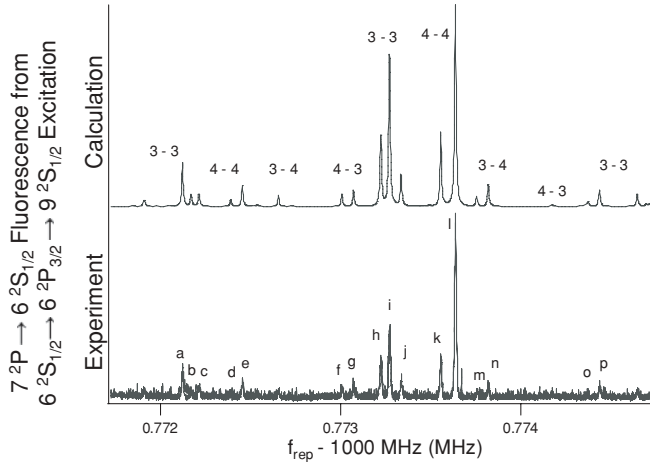


FIG. 8. The calculated spectrum (upper trace) and experimental signal (lower trace) of the $7P \rightarrow 6S$ fluorescence when the Cs atoms are excited to the $9S_{1/2}$ state through the $6P_{3/2}$ state. The peaks in the experimental spectrum labeled with letters were used in extracting the transition frequencies, as described in the text.

center-of-gravity frequency and hyperfine A constant of the $8S_{1/2}$ state of

$$\begin{aligned} \nu_{6S_{1/2}:8S_{1/2}} &= 729\,009\,798.86(19) \text{ MHz}, \\ A_{8S_{1/2}} &= 219.14(11) \text{ MHz}. \end{aligned}$$

These results are in good agreement with previous measurements of the $8S_{1/2}$ state, which are summarized in Table II.

C. Results for the $9S_{1/2}$ state

Figure 8 shows the spectrum obtained for the cascaded two-photon transition $6S_{1/2} \rightarrow 6P_{3/2} \rightarrow 9S_{1/2}$ and the calculated spectrum. This spectrum was collected by use of an 850-nm filter with a 10-nm passband for F1 and a 658-nm filter with a 10-nm passband for F2. The measurement of the $9S_{1/2}$ state through the $6P_{1/2}$ intermediate state was not possible because the complementary radiation at 635.5 nm was on the edge of the laser bandwidth.

The peaks a–p were used to determine the center-of-gravity frequency and the hyperfine A constant as described previously. The extracted center-of-gravity frequency is 806 761 363.380(58) MHz and the hyperfine A constant is 109.932(30) MHz. The χ^2 was 83 for 32 peaks.

The systematic effects due to ac-Stark shifts, Zeeman shifts, pressure shifts, and misalignment effects were investigated in the same way as they were for the $8S_{1/2}$ state. The systematic effects were studied by focusing on the three peaks labeled h, i, and j in Fig. 8, corresponding to transitions from the $F = 3$ ground-state hyperfine level to the $F'' = 3$ excited-state hyperfine level through the $F' = 2, 3,$ and 4 intermediate hyperfine levels.

The laser intensity for both transitions was varied. For the $6S_{1/2} \rightarrow 6P_{3/2}$ stage of the transition the variation was from ≈ 40 to 20 W/cm^2 and was spread over ≈ 4000 optical modes. A linear fit of the center-of-gravity frequency to the power gave a dependence of $-42(127) \text{ kHz}/P$, where P is the normalized

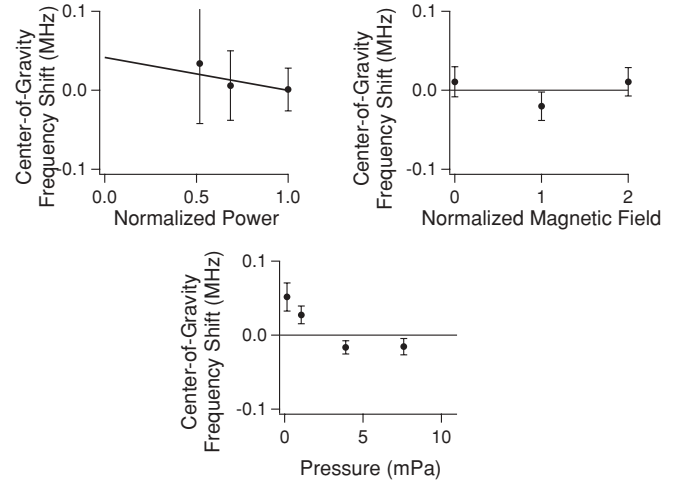


FIG. 9. The dependence of the center-of-gravity frequencies for the $6S_{1/2} \rightarrow 6P_{3/2} \rightarrow 9S_{1/2}$ state on the power (upper left), the magnetic field (upper right), and the Cs vapor pressure (bottom). The straight line for the power dependence is a weighted linear fit to the data. The vertical axis has been offset and centered so that the nominal operating point is at zero for the power-dependence plot. The magnetic field and pressure data are shown scattered about the weighted mean of the data. The power is plotted as a function of the fraction of the maximum power. The magnetic field is plotted as a function of the residual magnetic field, $\approx 50 \mu\text{T}$.

operating power. We therefore assign a 169-kHz uncertainty to the center-of-gravity frequency due to possible light shifts (Fig. 9). Similarly, for the hyperfine A constant we found a linear dependence consistent with zero slope, $21(58) \text{ kHz}/P$. We take 79-kHz uncertainty to be the uncertainty in the A constant due to possible ac-Stark shifts.

As with the $8S_{1/2}$ state, no discernible dependence of the frequency on the external magnetic field was observed (Fig. 9). Based on the scatter (standard deviation) of the data we arrive at an uncertainty of 18 kHz for the center-of-gravity frequency and 7 kHz for the hyperfine A constant.

Spectra were taken at four different temperatures of the vapor cell corresponding to Cs vapor pressures of 0.15, 1.06, 3.9, and 7.6 mPa. The dependence of the center-of-gravity frequency is shown in Fig. 9. There is evidence of a possible shift in the frequency with pressure. However, even at pressures that are 50 times larger than the nominal operating pressure, we see only a 67-kHz shift. We again use the standard deviation of the data to place a conservative limit on possible uncertainties due to pressure shifts and find a 34-kHz uncertainty in the optical frequency due to temperature dependent effects. A similar analysis for the hyperfine A constant gives an uncertainty due to temperature-dependent effects of 15 kHz.

An analysis of the frequency dependence on misalignment done in the same way as described previously yielded a 58-kHz uncertainty for the center-of-gravity frequency and 20 kHz for the hyperfine A constant.

The uncertainties to the center-of-gravity frequency and the hyperfine A constant are summarized in Table I.

TABLE II. Comparison of the center-of-gravity frequencies and hyperfine coupling constants measured in this work with previous measurements. All numbers are in megahertz. The uncertainties represent the standard error (68% confidence interval).

Measurement	Center-of-gravity frequency	Hyperfine constant A	Hyperfine constant B
$8S_{1/2}$			
This work	729 009 798.86(19)	219.14(11)	–
Fendel <i>et al.</i> [22]	729 009 799.020(26)	219.125(4)	–
Hagel <i>et al.</i> [21]	729 009 798.82(20)	219.12(1)	–
$9S_{1/2}$			
This work	806 761 363.38(19)	109.93(9)	–
Weber and Sansonetti [23]	806 761 372(8)	–	–
Farley <i>et al.</i> [29]	–	110.1(5)	–
Gupta <i>et al.</i> [30]	–	109.5(2.0)	–
$7D_{3/2}$			
This work	780 894 762.250(77)	7.386(15)	–0.18(16)
Weber and Sansonetti [23]	780 894 772(8)	–	–
Kortyna <i>et al.</i> [31]	–	7.36(3)	–0.1(2)
Auzinsh <i>et al.</i> [32]	–	7.4(2)	–
$7D_{5/2}$			
This work	781 522 153.68(10)	–1.717(15)	–0.18(52)
Weber and Sansonetti [23]	781 522 153(8)	–	–
Auzinsh <i>et al.</i> [32]	–	–1.56(9)	–

We arrive at final values for the center-of-gravity frequency for the $6S_{1/2} \rightarrow 9S_{1/2}$ transition and the hyperfine A constant of the $9S_{1/2}$ state of

$$\nu_{6S_{1/2};9S_{1/2}} = 806\,761\,363.38(19) \text{ MHz},$$

$$A_{9S_{1/2}} = 109.93(9) \text{ MHz}.$$

This is in good agreement with the previous measurements of this transition, which are summarized with other data in Table II, and improves on the center-of-gravity frequency by 2 orders of magnitude.

D. Results for the $7D_{3/2}$ state

The center-of-gravity frequency, magnetic dipole, and electric quadrupole hyperfine coupling constants for the $7D_{3/2}$ state were determined from the spectrum in Fig. 10. The filters used in collecting this spectrum were a 890-nm filter with a 10-nm passband for F1 and a 670-nm filter with a 30-nm passband for F2. This spectrum was taken by exciting Cs through the $6P_{1/2}$ intermediate state. Use of the $6P_{1/2}$ state eliminates possible transitions to the $7D_{5/2}$ state due to angular momentum selection rules. The groups consist of six peaks, corresponding to the $F \rightarrow F' = 3 \rightarrow F'' = 2, 3, 4$ and $F \rightarrow F' = 4 \rightarrow F'' = 3, 4, 5$ transitions. The 18 peaks labeled a through r in Fig. 10 were used to extract the frequency and hyperfine coupling constants.

The $7D$ state has $J > 1/2$ and, consequently, an electric quadrupole coupling denoted by the hyperfine B constant. Minimizing the $\chi^2(\nu, A, B)$ function defined by Eq. (10) with respect to the center-of-gravity frequency and the hyperfine A and B constants, we find a value for the center of gravity of 780 894 762.250(28) MHz, a hyperfine A constant value of 7.386(6) MHz, and a hyperfine B constant value of $-0.182(50)$. The χ^2 was 78 for 36 peaks.

The systematic effects were studied by focusing on the six peaks labeled g, h, i, j, k, and l in Fig. 10, corresponding to transitions from the $F = 3$ ground state. The laser intensity in both stages of the transition was varied. For the $6S_{1/2} \rightarrow 6P_{1/2}$ stage, the change in intensity ranged from ≈ 19 to $\approx 3 \text{ W/cm}^2$, spread over ≈ 4000 optical modes within the 10-nm (3.8-THz) filter bandwidth. The slope of the center-of-gravity frequency as a function of light power yields a dependence of 22(27) kHz (Fig. 11), corresponding to an uncertainty of 49 kHz. We find uncertainties due to ac-Stark shifts of 14 kHz for the A constant and 17 kHz for the B constant.

No effect of the external magnetic field was observed (Fig. 11), within the measurement uncertainties. Based on the

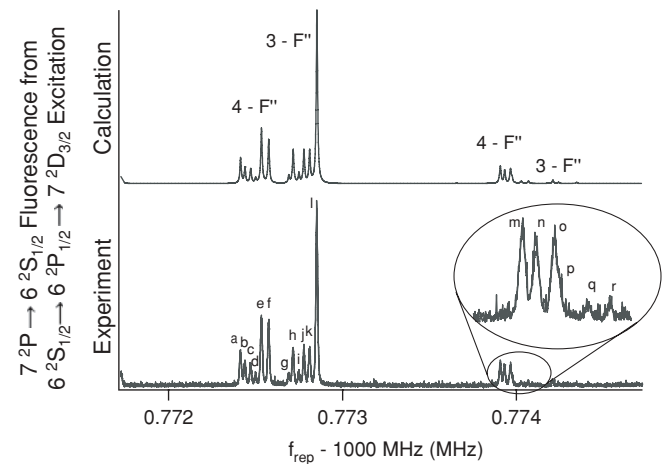


FIG. 10. The calculated spectrum (upper trace) and experimental signal (lower trace) of the $7P \rightarrow 6S$ fluorescence when the Cs atoms are excited to the $7D_{3/2}$ state through the $6P_{1/2}$ state. The peaks in the experimental spectrum labeled with letters were used in extracting the transition frequencies as described in the text.

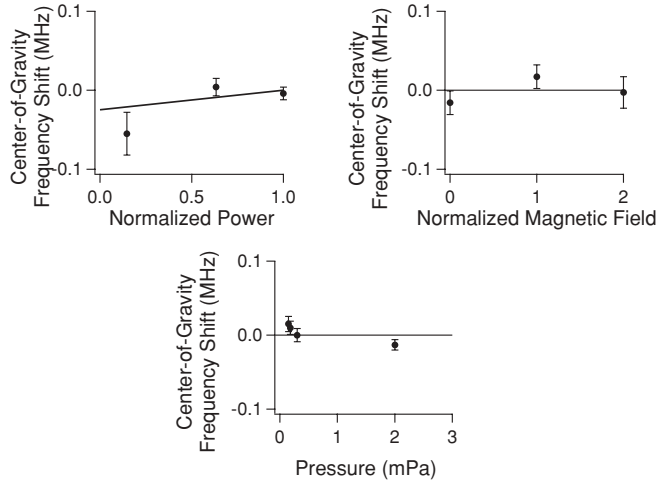


FIG. 11. The dependence of the center-of-gravity frequencies for the $6S_{1/2} \rightarrow 6P_{1/2} \rightarrow 7D_{3/2}$ transition on the power (upper left), the magnetic field (upper right), and the Cs vapor pressure (bottom). The straight line for the power dependence is a weighted linear fit to the data. The vertical axis has been offset and centered so that the nominal operating point is at zero for the power-dependence plot. The magnetic field and pressure data are shown scattered about the weighted mean of the data. The power is plotted as a function of the fraction of the maximum power. The magnetic field is plotted as a function of the residual magnetic field, $\approx 50 \mu T$.

scatter of the data, we assign uncertainties of 17, 3, and 17 kHz for the center-of-gravity frequency, the hyperfine A constant, and the hyperfine B constant, respectively.

Spectra were taken at four different temperatures of the vapor cell, corresponding to Cs vapor pressures of 0.15, 0.2, 0.3, and 2.0 mPa. As with the $9S_{1/2}$ state, there appears to be a small dependence of the center-of-gravity frequency as a function of the pressure in the cell, leading to a 28-kHz shift when the pressure is increased by a factor of ≈ 10 . However, since we fix the A and B constants, this serves as a maximal shift in the center-of-gravity frequency and we do not attempt to correct for this shift. We take the standard deviation as a conservative estimate of the error and assign an uncertainty of 12 kHz to the center-of-gravity frequency due to possible temperature-dependent effects. The hyperfine A constant shows no such dependence and the scatter is less than the uncertainty on the mean. We therefore use the uncertainty on the weighted mean of the data taken at different temperatures to arrive at an uncertainty of 1 kHz for the hyperfine A constant. For the hyperfine B constant we find an 11-kHz uncertainty (from the scatter of the data).

A theoretical analysis of the frequency dependence on misalignment similar to that described for the $8S_{1/2}$ state analysis yielded a 48-kHz uncertainty for the center-of-gravity frequency and uncertainties of 12 kHz for the hyperfine A constant and 143 kHz for the B constant. In addition, the effects of misalignment were investigated experimentally. Spectra of the six peaks labeled g, h, i, j, k, and l in Fig. 10 were taken at three different beam alignments. The degree of misalignment was characterized by the peak amplitude. Misalignment of the beams so that the peak amplitudes decreased by more

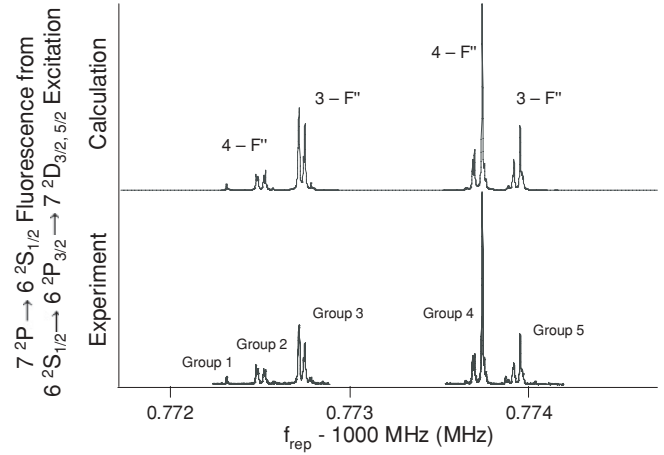


FIG. 12. The calculated spectrum (upper trace) of the $7P \rightarrow 6S$ fluorescence when the Cs atoms are excited to the $7D_{3/2,5/2}$ state. The experimental signal (lower trace) shows the $7P \rightarrow 6S$ fluorescence when the Cs atoms are excited to both the $7D_{3/2,5/2}$ states through the $6P_{3/2}$ state. In the experimental spectrum data are shown for only those regions where there was a signal.

than a factor of 2 resulted in no detectable change in the center-of-gravity, A constant, or B constant.

The uncertainties to the center-of-gravity frequency and the hyperfine A constant are summarized in Table I.

With the uncertainties from Table I we find

$$\begin{aligned} \nu_{6S_{1/2}:7D_{3/2}} &= 780\,894\,762.250(77) \text{ MHz}, \\ A_{7D_{3/2}} &= 7.386(15) \text{ MHz}, \\ B_{7D_{3/2}} &= -0.18(16) \text{ MHz}. \end{aligned}$$

These numbers are in good agreement with previous measurements, which are shown in Table II, and lead to a significant improvement in the knowledge of the center-of-gravity frequency.

E. Results for the $7D_{5/2}$ state

Figure 12 shows the experimental fluorescence spectra for excitation of the $7D_{3/2}$ and $7D_{5/2}$ states through the $6P_{3/2}$ state along with the calculated spectra for excitation to the $7D_{3/2}$ and $7D_{5/2}$ states. The spectrum was collected using an 850-nm filter with a 10-nm passband for F1 and a 700-nm filter with a 25-nm passband for F2. The close energy spacing of the $7D_{3/2}$ and $7D_{5/2}$ states did not allow for a selection of only one of the states when excited through the $6P_{3/2}$ state. However, because we were able to determine the $7D_{3/2}$ state energy and hyperfine splitting as described in Sec. IV D, we were able to fix the frequency of the $7D_{3/2}$ state from these measurements and use the spectrum shown in Fig. 12 to extract information about the $7D_{5/2}$ state. In addition, angular momentum considerations result in much stronger transition probabilities for the $6P_{3/2} \rightarrow 7D_{5/2}$ transition compared to the $6P_{3/2} \rightarrow 7D_{3/2}$ transition. To remove the effect of the overlap, we calculated the $7D_{3/2}$ spectrum through the $6P_{3/2}$ state using the values determined by the $6S_{1/2} \rightarrow 6P_{1/2} \rightarrow 7D_{3/2}$ excitation. Figure 13 shows the contribution of the transitions to the $7D_{3/2}$ to the fluorescence spectrum. We superposed that calculated spectrum on the experimental spectrum and

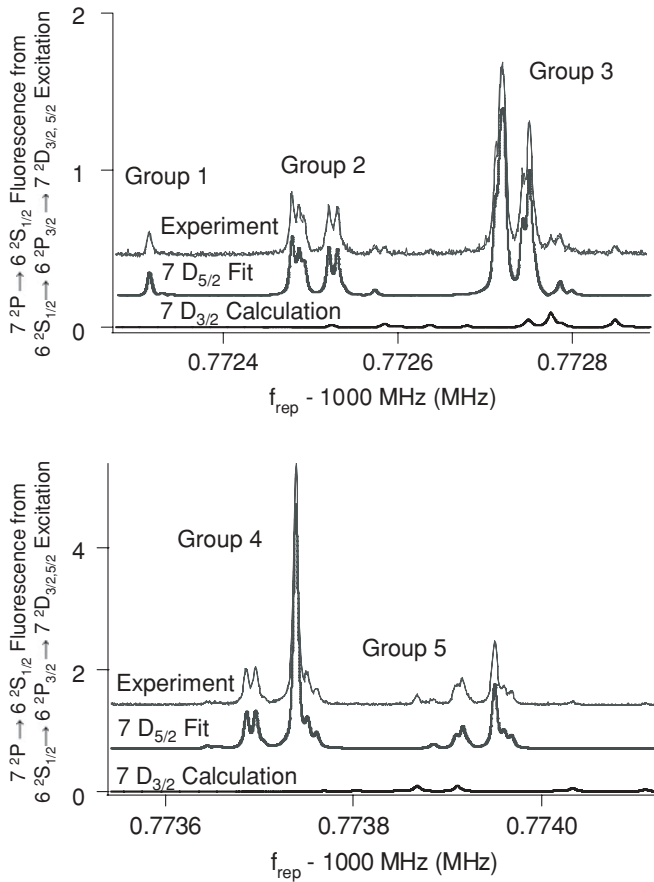


FIG. 13. The experimental spectrum (upper trace), fit to the $6S_{1/2} \rightarrow 6P_{3/2} \rightarrow 7D_{5/2}$ transition (middle trace), and the spectrum of the calculated contribution from the $6S_{1/2} \rightarrow 6P_{3/2} \rightarrow 7D_{3/2}$ transition (lower trace). Note that the vertical scales are different for the two figures.

adjusted the peak intensities to match the isolated $7D_{3/2}$ peaks. In this way we accounted for and removed the $7D_{3/2}$ parameters. To quantify the influence of the $7D_{3/2}$ state and estimate the uncertainty resulting from the overlapped spectra, we fit the spectra with and without subtracting the spectrum from the $7D_{3/2}$ state. We found a maximum deviation of 10 kHz in the center-of-gravity frequency of the $7D_{5/2}$ state, 1 kHz in the hyperfine A constant, and 30 kHz in the hyperfine B constant which we take to be the uncertainties due to this overlap. The contributions from the two transitions are separated in Fig. 13.

For a given ground-state hyperfine component F , there are nine distinct transitions due to the manifold of intermediate states and upper states. The five groups of peaks labeled in Fig. 12 were used to extract values for the center-of-gravity and hyperfine A and B constants. In group one, only three peaks were of sufficient amplitude to be fit. All nine peaks were fit in groups 3 and 5. Seven peaks were used in group two and six peaks in group four. From the fit to these 34 peaks we determined the center-of-gravity frequency to be $781\,522\,153.682(25)$ MHz and the hyperfine A and B constants were $-1.717(4)$ MHz and $-0.182(86)$ MHz, respectively. To improve the precision of the fits, we use scans with increasing frequency and decreasing frequency

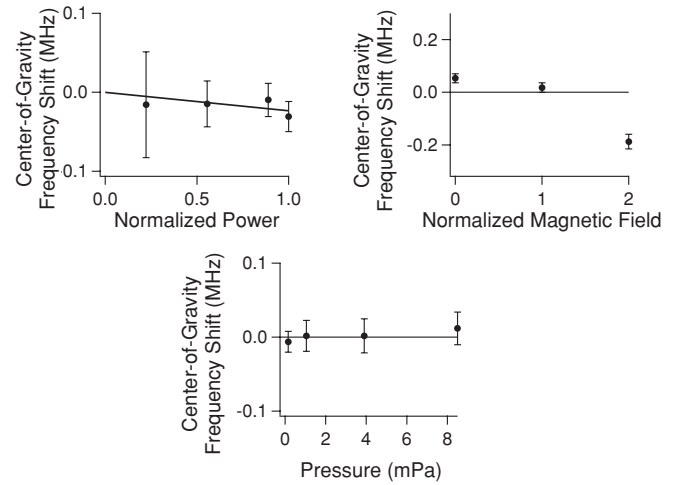


FIG. 14. The dependence of the center-of-gravity frequencies for the $6S_{1/2} \rightarrow 6P_{3/2} \rightarrow D_{5/2}$ transition on the power (upper left), the magnetic field (upper right), and the Cs vapor pressure (bottom). The straight line in the power dependence plot is a linear weighted fit to the data. The vertical axis has been offset and centered so that the nominal operating point is at zero. The power is plotted as a function of the fraction of the maximum power. The magnetic field is plotted as a function of the residual magnetic field.

simultaneously. The minimum χ^2 was 90 for 34 peaks prior to normalization.

The systematics were studied in the same way as with the previous states. We focused on group 4 of Fig. 13 due to its size and also the fact that there is very little contribution from the $7D_{3/2}$ state for this group. The optical intensity was varied for both stages of the transition. For the first stage the intensity over the 10-nm bandwidth was varied from ≈ 22 to ≈ 5 W/cm². Data were taken at cell temperatures corresponding to saturated vapor pressures of 0.15, 1.05, 3.9, and 8.5 mPa. The dependencies of the center-of-gravity on the varied parameters are shown in Fig. 14 and are summarized in Table I.

As with the previous transitions there was no significant shift arising from the light power. A linear fit gave a slope of $-23(62)$ kHz/ P , where P is the normalized operating power. This gives us an uncertainty of 85 kHz in the center-of-gravity frequency. We found uncertainties in the hyperfine A and B constants of 11 and 458 kHz, respectively.

Unlike the other transitions studied here, we did observe a dependence of the center-of-gravity on the magnetic field (Fig. 14). There was clear evidence of broadening in the peaks at the largest magnetic fields. We attribute the shift to a breakdown of the line-shape model as the line broadens coupled with the overlap of the peaks. In this case, we base our estimate of the uncertainty on the difference of the point taken at the zeroed field with the residual field and find an uncertainty of 35 kHz in the optical frequency. There is no evidence for a dependence of the extracted hyperfine A constant, and we find a magnetic-field uncertainty of 6 kHz for it. For the B constant we find an uncertainty of 125 kHz.

We see no clear evidence for any temperature-dependent effects. Using the larger of standard deviation or the uncertainty in the mean, we find uncertainties of 7, 1, and 38 kHz for the temperature-dependent uncertainties of the center-of-gravity

frequency, the hyperfine A constant, and the hyperfine B constant, respectively.

Applying these uncertainties we find

$$\nu_{6S_{1/2};7D_{5/2}} = 781\,522\,153.68(16) \text{ MHz},$$

$$A_{7D_{5/2}} = -1.717(15) \text{ MHz},$$

$$B_{7D_{5/2}} = -0.18(52) \text{ MHz}.$$

V. CONCLUSIONS

We have used the technique of velocity-selective two-photon excitation to measure the center-of-gravity frequencies and the hyperfine coupling constants for the $8S_{1/2}$, $9S_{1/2}$, $7D_{3/2}$, and $7D_{5/2}$ states of Cs. The results for all of the transitions are summarized and compared to other published experimental values in Table II. This technique has potential metrological applications for secondary frequency standards at optical wavelengths. At a more fundamental level, the hyperfine coupling measurements are valuable in improving atomic structure calculations. The measurement accuracy of multiple

transitions at significantly different wavelengths rivals that of cw laser spectroscopy techniques and demonstrates the versatility of DFCS.

Our measured transition frequencies are in good agreement with previous measurements, while achieving greater accuracy for the $9S_{1/2}$, $7D_{3/2}$, and $7D_{5/2}$ states. In these measurements the uncertainties were typically limited by signal-to-noise ratio and fitting uncertainties combined with uncertainties in the determination of the ac Stark shifts and geometrical factors.

ACKNOWLEDGMENTS

We thank Hugh Robinson for insightful advice and preparation of the Cs vapor cell. We are grateful to Jose Almaguer, Nate Newbury, and Todd Johnson for carefully reading the manuscript and providing valuable suggestions and discussions. One of us (V.M.) was supported in part by the DST(RSA) PDP through the National Metrology Institute of South Africa (NMISA). C.E.T. acknowledges partial support from the National Science Foundation through Grant No. PHY99-87984.

-
- [1] R. Teets, J. Eckstein, and T. W. Hänsch, *Phys. Rev. Lett.* **38**, 760 (1977).
 - [2] Y. V. Baklanov and V. P. Chebotayev, *Appl. Phys.* **12**, 97 (1977).
 - [3] J. N. Eckstein, A. I. Ferguson, and T. W. Hänsch, *Phys. Rev. Lett.* **40**, 847 (1978).
 - [4] M. M. Salour, *Rev. Mod. Phys.* **50**, 667 (1978).
 - [5] T. W. Hänsch, S. A. Lee, R. Wallenstein, and C. Wieman, *Phys. Rev. Lett.* **34**, 307 (1975).
 - [6] T. W. Hänsch and N. C. Wong, *Metrologia* **16**, 101 (1980).
 - [7] D. J. Jones, S. A. Diddams, J. K. Ranka, A. Stentz, R. S. Windeler, J. L. Hall, and S. T. Cundiff, *Science* **288**, 635 (2000).
 - [8] R. Holzwarth, T. Udem, T. W. Hänsch, J. C. Knight, W. J. Wadsworth, and P. S. J. Russell, *Phys. Rev. Lett.* **85**, 2264 (2000).
 - [9] M. C. Stowe, M. J. Thorpe, A. Pe'er, J. Ye, J. E. Stalnaker, V. Gerginov, and S. A. Diddams, *Advances in Atomic, Molecular, and Optical Physics* (Academic Press, New York, 2008), Vol. 55.
 - [10] C. S. Wood, S. C. Bennett, D. Cho, B. P. Masterson, J. L. Roberts, C. E. Tanner, and C. E. Wieman, *Science* **275**, 1759 (1997).
 - [11] S. C. Bennett and C. E. Wieman, *Phys. Rev. Lett.* **82**, 2484 (1999).
 - [12] J. Guena, M. Lintz, and M. A. Bouchiat, *J. Opt. Soc. Am. B* **22**, 21 (2005).
 - [13] S. A. Murthy, D. Krause, Z. L. Li, and L. R. Hunter, *Phys. Rev. Lett.* **63**, 965 (1989).
 - [14] H. S. Nataraj, B. K. Sahoo, B. P. Das, and D. Murkherjee, *Phys. Rev. Lett.* **101**, 033002 (2008).
 - [15] A. Wicht, J. M. Hensley, E. Sarajlic, and S. Chu, *Phys. Scr. T* **102**, 82 (2002).
 - [16] V. Gerginov, K. Calkins, C. E. Tanner, J. J. McFerran, S. Diddams, A. Bartels, and L. Hollberg, *Phys. Rev. A* **73**, 032504 (2006).
 - [17] V. Gerginov, A. Derevianko, and C. E. Tanner, *Phys. Rev. Lett.* **91**, 072501 (2003).
 - [18] A. J. Leggett, *Rev. Mod. Phys.* **73**, 307 (2001).
 - [19] R. Wynards and S. Weyers, *Metrologia* **42**, S64 (2005).
 - [20] D. Budker and M. V. Romalis, *Nat. Phys.* **3**, 227 (2007).
 - [21] G. Hagel, C. Nesi, L. Jozefowski, C. Schwob, F. Nez, and F. Biraben, *Opt. Commun.* **160**, 1 (1999).
 - [22] P. Fendel, S. D. Bergeson, T. Udem, and T. W. Hänsch, *Opt. Lett.* **32**, 701 (2007).
 - [23] K.-H. Weber and C. J. Sansonetti, *Phys. Rev. A* **35**, 4650 (1987).
 - [24] T. M. Fortier, A. Bartels, and S. A. Diddams, *Opt. Lett.* **31**, 1011 (2006).
 - [25] V. Gerginov, C. E. Tanner, S. Diddams, A. Bartels, and L. Hollberg, *Phys. Rev. A* **70**, 042505 (2004).
 - [26] W. Demtröder, *Laser Spectroscopy: Basic Concepts and Instrumentation*, 3rd ed. (Springer-Verlag, New York, 2003)
 - [27] I. I. Sobelman, *Atomic Spectra and Radiative Transitions*, 2nd ed. (Springer-Verlag, New York, 1996)
 - [28] A. Corney, *Atomic and Laser Spectroscopy* (Oxford University Press, New York, 1979).
 - [29] J. Farley, P. Tsekeris, and R. Gupta, *Phys. Rev. A* **15**, 1530 (1977).
 - [30] R. Gupta, W. Happer, L. K. Lam, and S. Svanberg, *Phys. Rev. A* **8**, 2792 (1973).
 - [31] A. Kortyna, V. Fiore, and J. Farrar, *Phys. Rev. A* **77**, 062505 (2008).
 - [32] M. Auzinsh, K. Bluss, R. Ferber, F. Gahbauer, A. Jarmola, M. S. Safronova, U. I. Safronova, and M. Tamanis, *Phys. Rev. A* **75**, 022502 (2007).